



**Experimental Determination of AH-64 Apache  
Tailshaft Hanger Bearing Vibration Characteristics  
with Seeded Faults**

**by Brian Dykas, Timothy Krantz, Harry Decker, and David Lewicki**

**ARL-TR-4865**

**June 2009**

## **NOTICES**

### **Disclaimers**

The findings in this report are not to be construed as an official Department of the Army position unless so designated by other authorized documents.

Citation of manufacturer's or trade names does not constitute an official endorsement or approval of the use thereof.

Destroy this report when it is no longer needed. Do not return it to the originator.

# **Army Research Laboratory**

NASA Glenn, Cleveland, OH, 44135-3191

---

**ARL-TR-4865**

**June 2009**

---

## **Experimental Determination of AH-64 Apache Tailshaft Hanger Bearing Vibration Characteristics with Seeded Faults**

**Brian Dykas, Timothy Krantz, Harry Decker, and David Lewicki**  
Vehicle Technology Directorate, ARL

# REPORT DOCUMENTATION PAGE

*Form Approved*  
OMB No. 0704-0188

Public reporting burden for this collection of information is estimated to average 1 hour per response, including the time for reviewing instructions, searching existing data sources, gathering and maintaining the data needed, and completing and reviewing the collection information. Send comments regarding this burden estimate or any other aspect of this collection of information, including suggestions for reducing the burden, to Department of Defense, Washington Headquarters Services, Directorate for Information Operations and Reports (0704-0188), 1215 Jefferson Davis Highway, Suite 1204, Arlington, VA 22202-4302. Respondents should be aware that notwithstanding any other provision of law, no person shall be subject to any penalty for failing to comply with a collection of information if it does not display a currently valid OMB control number.

**PLEASE DO NOT RETURN YOUR FORM TO THE ABOVE ADDRESS.**

<b>1. REPORT DATE (DD-MM-YYYY)</b> June 2009		<b>2. REPORT TYPE</b> Final		<b>3. DATES COVERED (From - To)</b> 2007 to 2008	
<b>4. TITLE AND SUBTITLE</b> Experimental Determination of AH-64 Apache Tailshaft Hanger Bearing Vibration Characteristics with Seeded Faults				<b>5a. CONTRACT NUMBER</b>	
				<b>5b. GRANT NUMBER</b>	
				<b>5c. PROGRAM ELEMENT NUMBER</b>	
<b>6. AUTHOR(S)</b> Brian Dykas, Timothy Krantz, Harry Decker, and David Lewicki				<b>5d. PROJECT NUMBER</b>	
				<b>5e. TASK NUMBER</b>	
				<b>5f. WORK UNIT NUMBER</b>	
<b>7. PERFORMING ORGANIZATION NAME(S) AND ADDRESS(ES)</b> U.S. Army Research Laboratory NASA Glenn ATTN: RDRL-VTP Cleveland, OH 44135-3191				<b>8. PERFORMING ORGANIZATION REPORT NUMBER</b>  ARL-TR-4865	
<b>9. SPONSORING/MONITORING AGENCY NAME(S) AND ADDRESS(ES)</b> U.S. Army Research Laboratory 2800 Powder Mill Road Adelphi, MD 20783-1197				<b>10. SPONSOR/MONITOR'S ACRONYM(S)</b>	
				<b>11. SPONSOR/MONITOR'S REPORT NUMBER(S)</b>	
<b>12. DISTRIBUTION/AVAILABILITY STATEMENT</b> Approved for public release; distribution unlimited.					
<b>13. SUPPLEMENTARY NOTES</b>					
<b>14. ABSTRACT</b> A series of seeded fault experiments are conducted to evaluate the characteristics of degraded AH-64 Apache helicopter forward hanger bearings, which support the tail rotor drive shaft. This bearing is one of a handful of maintenance-intensive components originally identified for condition-based maintenance proof of principle. Several fault modes are simulated in the test specimens including salt water corrosion, sand contamination, and trench flaws on the races. The vibration characteristics of the faulted bearings are then recorded in a component-level bearing test stand, and analyzed to corroborate or modify current fault detection methodology in the aircraft. For the bearings with substantial amounts of damage or removed material, the vibration response showed increase content in a portion of the spectrum not monitored by the condition indicators now in use. Impact experiments suggest this is a result of the bearing vibration exciting the hanger assembly natural frequencies.					
<b>15. SUBJECT TERMS</b> Bearings, grease lubrication, seeded fault, vibration, prognostics and diagnostics					
<b>16. SECURITY CLASSIFICATION OF:</b>			<b>17. LIMITATION OF ABSTRACT</b>  UU	<b>18. NUMBER OF PAGES</b>  30	<b>19a. NAME OF RESPONSIBLE PERSON</b> Brian Dykas
<b>a. REPORT</b> Unclassified	<b>b. ABSTRACT</b> Unclassified	<b>c. THIS PAGE</b> Unclassified			<b>19b. TELEPHONE NUMBER (Include area code)</b> (216) 433-6058

---

## Contents

---

<b>List of Figures</b>	<b>iv</b>
<b>Acknowledgments</b>	<b>v</b>
<b>1. Introduction</b>	<b>1</b>
<b>2. Experimental Methods</b>	<b>1</b>
<b>3. Baseline (Healthy) Experiments</b>	<b>4</b>
<b>4. Bearing Seeded Fault Experiments</b>	<b>5</b>
4.1 EDM Trench Simulated Spalls.....	6
4.2 Corrosion.....	8
4.3 Sand Contamination.....	12
4.4 Other Seeded Faults.....	15
<b>5. Concluding Remarks</b>	<b>16</b>
<b>6. References</b>	<b>18</b>
<b>Appendix. Natural Frequency Identification in the Hanger Assembly</b>	<b>19</b>
<b>List of Symbols, Abbreviations, and Acronyms</b>	<b>21</b>
<b>Distribution List</b>	<b>22</b>

---

## List of Figures

---

Figure 1. Diagram of rig layout. ....	2
Figure 2. Mounting stand showing hanger bearing assembly bolted to it. ....	2
Figure 3. Orientations of two accelerometers attached to the hanger assembly .....	3
Figure 4. Condition indicator values for six baseline bearings, (a) shock pulse energy, (b) bearing energy, (c) amplitude demodulation, and (d) one per revolution.....	5
Figure 5. (a) Photograph and (b) Profile measurement of as-machined 0.030 inch wide flaw cross section for 026-ARL-TM.....	6
Figure 6. Time traces of (a) RMS acceleration signal and (b) HB Shock Pulse Energy CI for medium trench spall size.....	7
Figure 7. FFT of bearing vibration for medium trench spall size, compared with baseline spectrum.....	8
Figure 8. Photographs of characteristic grease appearance for each attempted method to corrode the bearing, (a) salt water mixed into grease, (b) reduced grease, salt water injected directly into bearing. ....	9
Figure 9. Time traces of broadband RMS vibration for (a) 018-ARL-SW and (b) 019-ARL-RS. ....	10
Figure 10. Comparison of FFT of accelerometer signal for corrosion seeded fault bearings: 019 with visible corrosion versus 018 which did not exhibit damage despite salt-water mixed into grease. ....	10
Figure 11. Condition indicator trends for corrosion test 019, (a) shock pulse energy and (b) HB energy. ....	11
Figure 12. Photographs of corrosion damage to bearing 019-ARL-RS after post-test disassembly.....	12
Figure 13. Time traces of (a) acceleration, (b) torque, and (c) HB energy CI, for a test with fine sand (012-ARL-FS). ....	13
Figure 14. Snapshots of FFT of acceleration signal at several points during 012-ARL –FS (hh:mm:ss in legend).....	14
Figure 15. Time traces of broadband RMS vibration for other sand contaminated bearings – (a) 011-ARL-CS, (b) 014-ARL-CS, and (c) 015-ARL-FS .....	14
Figure 16. Single simulated spall in center of race.....	15
Figure 17. Grease appearance after 1600 hr of elevated temperature (accelerated life) operation. ....	16

---

## **Acknowledgments**

---

The authors would like to express gratitude for the technical direction and programmatic support provided by the Army's Aviation Engineering Directorate throughout the course of this study. In addition, Dr. Romeo del Rosario and his colleagues at the Army Research Laboratory, Sensors and Electron Devices Directorate, are also thanked for providing additional support under an Army Technology Objective for Prognostics and Diagnostics. The authors also wish to thank researchers and technicians at NASA Glenn Research Center for their collaboration in this work.

INTENTIONALLY LEFT BLANK.

---

## 1. Introduction

---

The U.S. Army has identified condition-based maintenance (CBM) practices as having the potential to reduce logistics requirements for its vehicles and other materiel solutions. Army aviation leads this effort due to the high airframe and logistics costs. The criticality of component health drives conservative time-based maintenance practices, which may be enhanced and optimized through the use of component health monitoring (1).

Instrumenting mechanical and structural components is a first step to providing information necessary for health monitoring. However, an accurate understanding of failure physics and probability is necessary for the development of robust algorithms that can reliably detect incipient failure while minimizing false positives. In the case of Army helicopters, several drivetrain components are already instrumented (2), and proper data collection, manipulation, and decision making can allow more intelligent condition monitoring and fleet maintenance management.

For this work, a seeded fault approach is taken with the tailshaft hanger bearing from the Army's AH-64 Apache attack helicopter, initially targeted as part of the CBM proof of principle process (3). Vibration signatures from healthy and faulted bearings are compared to determine how reliably each failure mode can be detected using currently fielded condition indicators, as well as providing additional data for future algorithm development. This empirical approach helps to validate physics-based failure modeling.

---

## 2. Experimental Methods

---

Investigation of vibration behavior of baseline and faulted bearings is primarily conducted on a component-level stand adapted to run hanger bearings in the forward hanger assembly from the aircraft. This test rig consists of a variable-speed electric motor, belt and pulley system, and shafting system attached to a heavy machine base that rests on a large bedplate. A schematic of the configuration and some dimensions are provided in figure 1. It was necessary to build a stand to mount the Apache forward hanger bearing assembly and maintain a 43 cm (17 in) centerline height for the test bearing consistent with the existing rig bearing pedestals. The test bearing mounting stand is an assembly of aluminum pieces bolted and welded together (figure 2). The test rig shafting was aligned using a laser alignment system, and the rig shaft was balanced. The radial load on the test bearing is roughly half the weight of the shaft, or about 55 N (12 lb). The bearing is expected to see relatively light loads in the aircraft as well, although they are expected to be somewhat higher than experienced in this component test stand. This

experimental setup and general seeded fault experiment methodology follows that described by Krantz et al. (4).

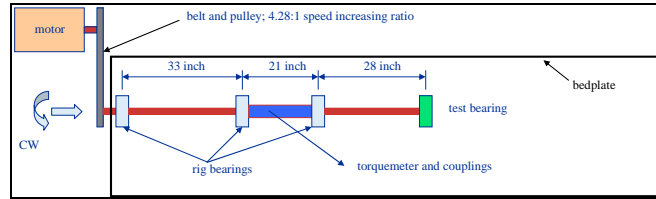


Figure 1. Diagram of rig layout.

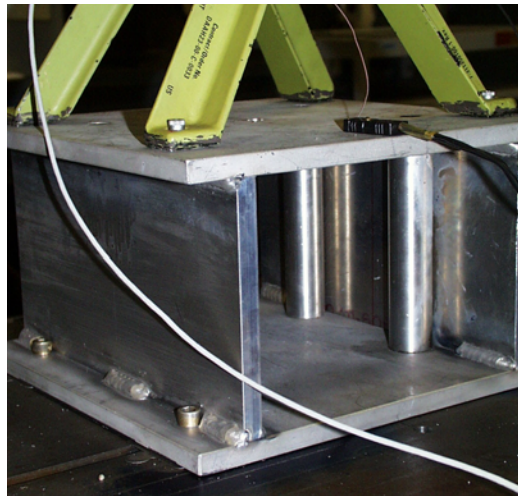


Figure 2. Mounting stand showing hanger bearing assembly bolted to it.

The AH-64 hanger bearing is a single row, double sealed, all-steel, grease-packed ball bearing lubricated with grease that conforms to MIL-PRF-81322 specification. It is designated by National Stock Number 3120-01-171-3942, "Bearing, plain, spherical." It has a riveted cage and nominally operates at approximately 4860 rev/min, with a corresponding DN of around 0.2 million. Details of the position of this bearing within the AH-64 drivetrain can be found in reference 5. A recent airworthiness release has increased time between overhaul for both forward and aft hanger bearings from 2500 to 2750 hr for aircraft with continuous diagnostic monitoring (6).

The test bearing was instrumented with two separate accelerometers mounted on the Apache hanger bearing assembly. One accelerometer was that supplied with a Vibration Management Enhancement Program (VMEP) system, to mimic the on-wing instrumentation (7). This sensor was located at the 9 o'clock position and is mounted in the same manner as on the aircraft (figure 3). The second accelerometer was a high frequency response accelerometer attached to a separate data acquisition system, located at the 3 o'clock position, and it was attached by drilling and tapping the bearing hanger assembly to accept a mounting stud. This allows for collection of VMEP data as well as high frequency raw data for further analysis and manipulation.

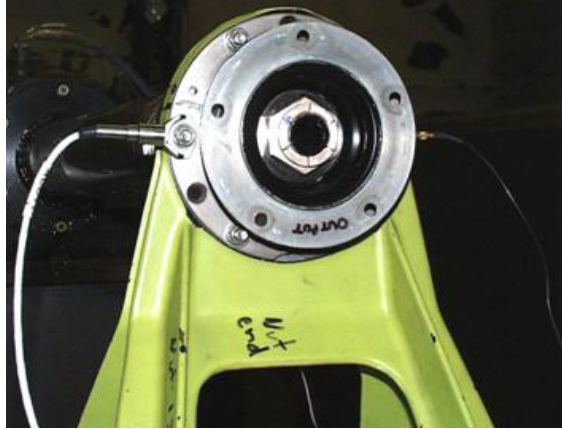


Figure 3. Orientations of two accelerometers attached to the hanger assembly

The VMEP HUMS system was used to measure bearing acceleration and quantify bearing operation through reported Condition Indicators (CIs). The algorithms used to calculate these CIs in the component-level laboratory tests are the same as those monitored on the VMEP-equipped aircraft—typically these are filtered portions of the vibration spectrum that are expected to respond to various physical faults (8). The four condition indicators monitored for this work were used to assess if fielded condition monitoring systems would be able to detect faults of the type described here. A basic description of each CI is given below.

The first computed CI is the bearing shock pulse energy (“Fwd HB Shock Pulse Energy”), with units of acceleration in g. It is the root mean square of the 12,000–17,500 Hz band of the asynchronous vibration spectrum, giving a measure of the high frequency energy.

The second CI is the bearing energy, (“Fwd HB Energy”), with units of acceleration in g. It is the root mean square of the 100–1100 Hz band of the asynchronous vibration spectrum, rejecting the second harmonic band of 161–163 Hz.

The third CI is the once per revolution vibration (“Fwd HB 1R Vib”), having units of inches per second. It is the synchronous vibration of the tail rotor drive shaft measured at the forward hanger bearing. A relatively wide band from 60–100 Hz is included to compute this condition indicator.

The final CI is the amplitude demodulated bearing vibration (“Fwd HB AMD Brg Vib”), having units of acceleration in g. It is the peak vibration within the range of 170–970 Hz from the amplitude demodulated spectrum (0–1172 Hz, 400 pts, 10 avgs, Flattop window).

The operating speed to match operation on the aircraft was 4860 rev/min. After reaching this operating speed (usually within 1–2 min from start), the bearing was allowed to run for approximately 15 min to reach a steady state temperature before taking 10–12 vibration snapshots. When the data acquisition was completed, the rig was slowly decelerated to a stop,

for a total test time of 15–30 min. This procedure was generally followed where possible, although this was altered to shorten or lengthen certain experiments as required.

Baseline measurements were made on healthy bearings in order to establish healthy vibration signatures and CI levels. These are useful for comparison to results obtained from other component-level test rigs, as well as system-level stands and aircraft data. The faulted bearings were then tested and compared to the baseline data to determine if the faults were distinguishable from normal bearings.

---

### **3. Baseline (Healthy) Experiments**

---

A series of experiments was conducted on as-received bearings to establish the baseline signatures. Generally speaking, it is difficult to infer the vibration characteristics of a faulted component in an aircraft based solely on the results of component-level or even system-level test stands. Baseline experiments help establish a context under which the seeded fault vibration experiments can be evaluated.

A total of six unfaulted bearings were run while condition indicators were tracked. It is noteworthy that these bearings were run at 4815 rev/min rather than the 4860 rev/min speed at which the faulted bearings were run. Based on the condition indicator definitions however, this approximately 1% speed error had little effect on the calculated values. All four condition indicators showed very low values in the healthy bearings when compared to the caution and exceedance values, but there was also a substantial amount of scatter. Plots of these values obtained for all four CIs and across all six baseline bearings are given in figure 4.

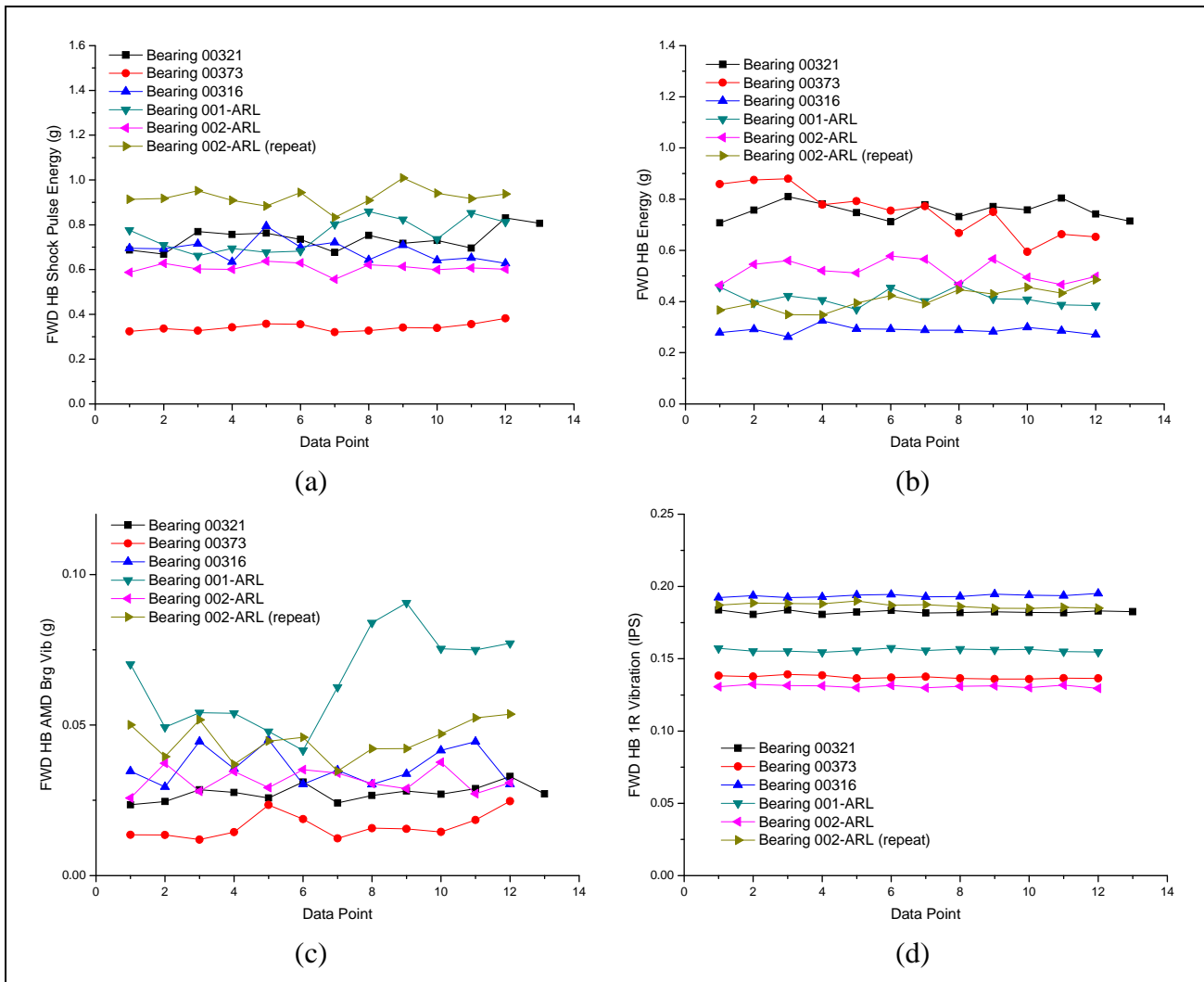


Figure 4. Condition indicator values for six baseline bearings, (a) shock pulse energy, (b) bearing energy, (c) amplitude demodulation, and (d) one per revolution.

## 4. Bearing Seeded Fault Experiments

In a typical experiment, a fault was introduced to the test bearing, which was installed in the component rig for the experiment. A single test of each bearing specimen was generally conducted where vibration characteristics, including both raw data and calculated condition indicators, are monitored and recorded from the VMEP and facility systems. This method provides an immediate indication of whether the CIs programmed on the aircraft will respond to the failure modes that are simulated by the seeded faults. It also allows for further analysis of the raw acceleration data using different or novel signal processing methods. In many cases, condition indicator values did not respond clearly to the introduced flaws, although some evidence of the damage could be ascertained from the root mean square (RMS) acceleration trace or additional energy in certain portions of the frequency domain.

The three seeded faults discussed here are: simulated spall line on the inner race, corrosion damage from introduction of salt water, and sand contamination. Additional fault modes were investigated as part of this study but detailed results are not discussed in this report.

#### 4.1 EDM Trench Simulated Spalls

To simulate a spall on the bearing, a single trench was created using electric discharge machining (EDM) in the ball track on the inner race. Three bearings were prepared with different trench profiles to evaluate the effect of flaw size on vibration signature. Both seals were removed from each bearing and the rivets were pressed out of the cage. The bearing was disassembled and cleaned in an ultrasonic bath using a degreasing agent. The races were then cleaned with alcohol and covered with a water displacing spray to protect the components from corrosion until the flaw was introduced and the bearings reassembled.

The trenches were specified to have a semicircular profile, oriented perpendicular to the direction of ball travel, conforming to the ball track and extending all the way across it. The trench depths were about 0.008, 0.015, and 0.023 in, with corresponding widths of approximately 0.015, 0.030, and 0.045 in.

After the trenches were machined into the inner races, the as-machined flaws are photographed and measured using stylus-based profilometry to verify the dimensions. For the intermediate flaw size, (specimen 026-ARL-TM), this photograph and profile are given in figure 5. After documenting the flaw, each bearing was reassembled and the cage was fastened together with small screws and nuts, secured with thread locking compound. A standard charge of MIL-PRF-81322 grease was introduced into the bearing and the seals were reinstalled.

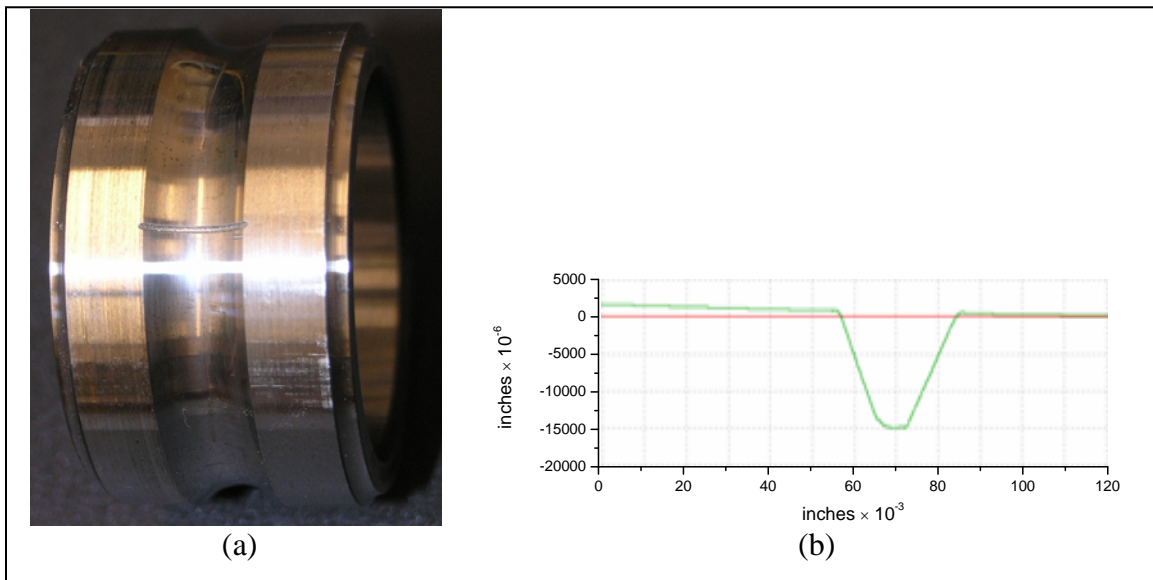


Figure 5. (a) Photograph and (b) Profile measurement of as-machined 0.030 inch wide flaw cross section for 026-ARL-TM.

For all three flaw sizes, the respective tests showed elevated overall vibration and an increase in the “Fwd HB Shock Pulse Energy,” condition indicator, as shown in figure 6. Other condition indicators did not respond as strongly when compared to the baseline (healthy) bearings. Because of the abrupt or sharp nature of the trench flaws, it is not surprising that the condition indicator tracking the highest frequency band responds most strongly to the flaw. However, among the three flaw sizes it should be noted that the condition indicator values did not necessarily trend with flaw size. The intermediate flaw size showed the largest increase in shock pulse energy and the largest “steady” RMS vibration values. It is unclear whether this result is due to poor repeatability or the nature of the flaw, but further investigation was not conducted during the course of testing.

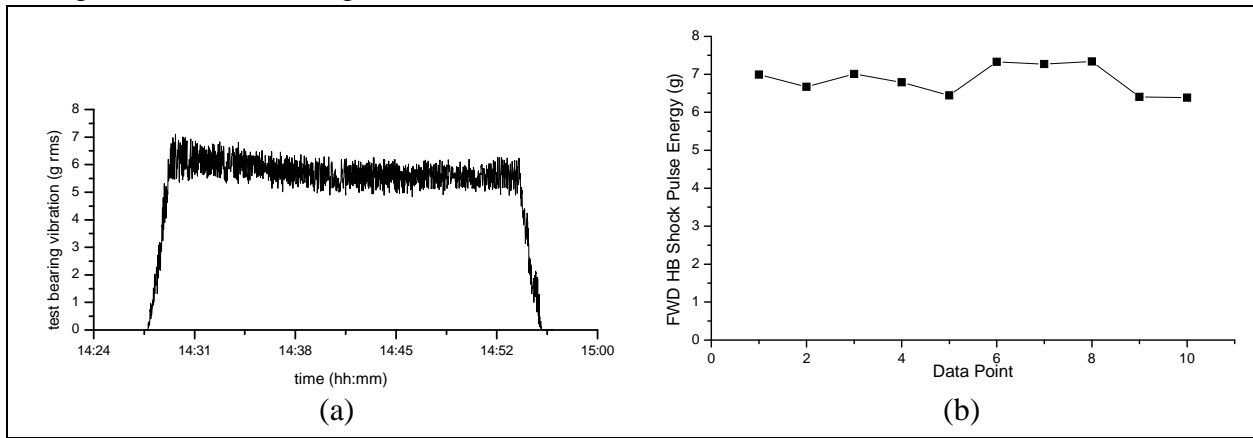


Figure 6. Time traces of (a) RMS acceleration signal and (b) HB Shock Pulse Energy CI for medium trench spall size.

It is notable that for all flaw sizes, irrespective of the specific RMS vibration or CI values, an fast Fourier transform (FFT) of the vibration signal showed two distinct bands of increased vibration compared to the baseline bearings. These bands were centered around approximately 2000 Hz and 5200 Hz, where figure 7 shows the spectral response of the bearing with the intermediate trench size. The baseline bearings also show content in these bands, as evidenced by the FFT of bearing 002 in figure 7, and appear to correspond with some of the natural frequencies of the hanger assembly. These natural frequencies are examined in more detail in the appendix.

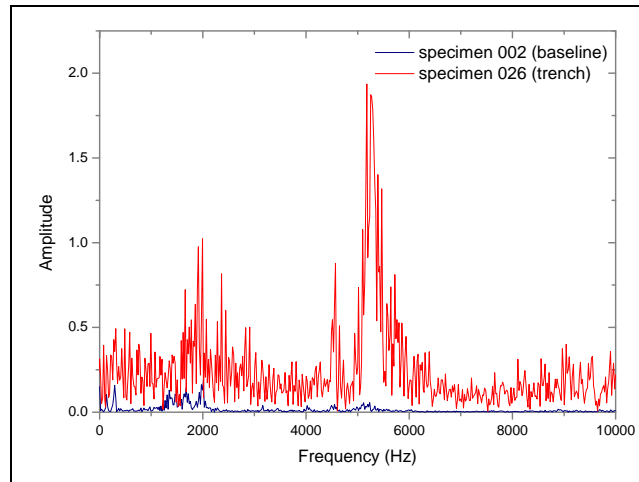


Figure 7. FFT of bearing vibration for medium trench spall size, compared with baseline spectrum.

## 4.2 Corrosion

The two methods employed in an attempt to seed corrosion into the test bearings included a mixture of grease and salt water, and a removal of most of the grease with a subsequent injection of salt water directly into the bearing. Salt water was first prepared by mixing 118 g of deionized water with 7 g of American Chemical Society certified NaCl.

Using the prepared salt water, a mixture of grease and salt-water was prepared by warming 100 cm<sup>3</sup> (cc) of grease to a temperature of 120 °F and adding 11 cc of the salt water. This was then mixed thoroughly by mechanical stirring, and sealed in a tightly capped container to prevent evaporation of the water until the bearings were prepared.

Three bearings were prepared using this mixture. The bearing seals were removed followed by degreasing and ultrasonic cleaning to remove the original grease from the bearings. The bearings were then flushed with clean water and immediately dried with forced air, followed by an immediate cleaning with alcohol. The bearings were then packed with 10–12 cc (standard charge) of the salt-water contaminated grease, and sealed in individual specimen bags to prevent evaporation of the water until the bearings were tested (about three months later). The test runs of these three bearings contain a “-SW” to designate salt water contaminated grease.

The second corrosion fault method included removal of most of the accessible grease by a small spatula, in the amount of about 75% of the nominal grease charge. Three bearings were prepared using this procedure. For each bearing, both seals were taken off to allow removal of grease from both sides of the bearing. After removal, one seal was reinstalled and 2 cc of the salt water mixture (118 g H<sub>2</sub>O/7g NaCl) was injected into the bearing with a syringe while turning slowly so that the water would be distributed in the bearing. The second seal was then reinstalled and the bearing was immediately placed in a specimen bag to prevent evaporation of the water until

the bearing was tested (approximately three months later). These samples were labeled with “-RS” to designate reduced grease, salt water contaminated.

When the bearings were to be tested, the seals were removed for inspection of the bearing surfaces for signs of corrosion. For the bearings which had a full charge the salt-water and grease mixture, the appearance after the three month wait period was not significantly different than that after initial preparation (figure 8a). However, the salt-water and grease mixture did have a slightly lighter color than the fresh grease, which had a deeper red appearance. Rotation of the bearings by hand revealed no discernible change in resistance or smoothness.

On the other hand, pretest inspections of bearings that had much of the original grease charge removed, followed by direct injection of salt water, revealed substantial corrosion and altered grease appearance, as shown in figure 8b. Brown and rust-colored grease was characteristic of all three bearings prepared in this manner, and rotation by hand was very rough, and in two of these samples, the components were locked together to some degree and some manual force was required to break the bearing free. In the case of both methods, all bearings prepared according to the same procedure had a similar appearance.

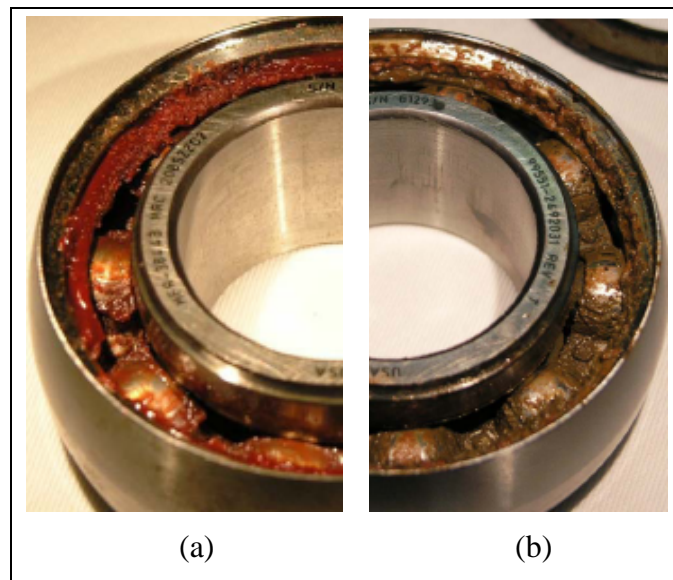


Figure 8. Photographs of characteristic grease appearance for each attempted method to corrode the bearing, (a) salt water mixed into grease, (b) reduced grease, salt water injected directly into bearing.

For all three of the bearings prepared with a salt-water and grease mixture, initial review of the data showed no obvious increase in broadband RMS vibration or CI levels beyond the baseline. For the salt-water injected bearings however, an order of magnitude increase in the RMS vibration signal indicated the severity of the damage. The high level of vibration in these samples resulted in a small amount of clipping of the raw vibration signal, so the plots of acceleration in both time and frequency domains (figures 9 and 10, respectively) are expected to

have some error attributed to that. The independent VMEP accelerometer sensor range and configuration were set much higher and the calculated condition indicator values did not appear to be affected by the clipping. The comparison of vibration time traces for 018-ARL-SW and 019-ARL-RS is shown in figure 9, with the order of magnitude difference corroborating the pretest inspection which suggested damage would be present in 019, but not in 018. A comparison of FFT snapshots of the acceleration signal from each of these experiments appears in figure 10, and further demonstrates where the vibration energy is most evident in the frequency domain. Here again, two distinct bands can be seen in the corrosion damaged 019 bearing, one centered at about 2000 Hz and the other centered at approximately 5200 Hz. As described in comparison to the trench flaw bearings, baseline bearings also exhibit energy in these frequency bands but not necessarily to the same relative magnitude.

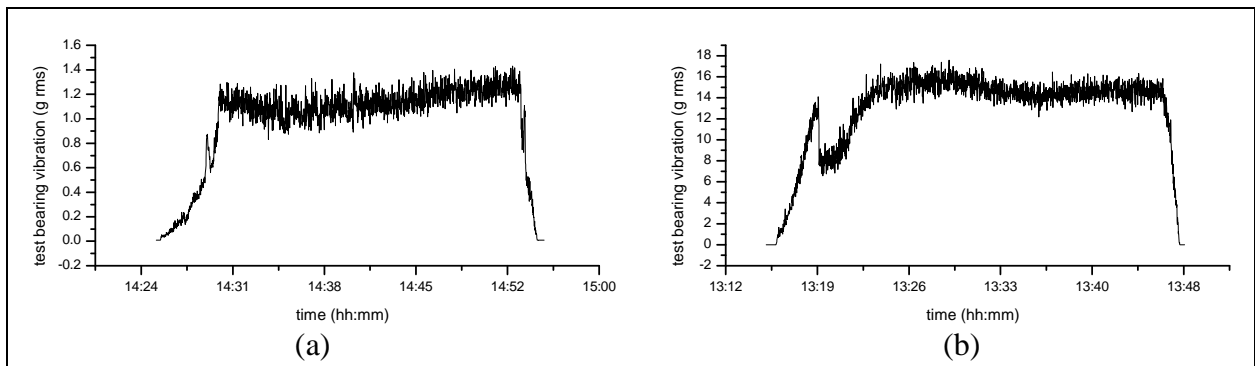


Figure 9. Time traces of broadband RMS vibration for (a) 018-ARL-SW and (b) 019-ARL-RS.

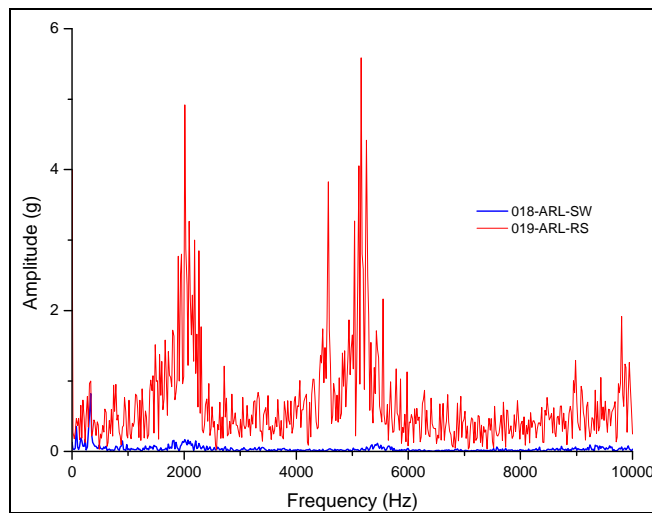


Figure 10. Comparison of FFT of accelerometer signal for corrosion seeded fault bearings: 019 with visible corrosion versus 018 which did not exhibit damage despite salt-water mixed into grease.

For the salt-water injected bearings that exhibited corrosion damage, two of the VMEP condition indicators responded significantly to the damage – “Fwd HB Shock Pulse Energy,” and “Fwd HB Energy.” In all three cases, caution or exceedance levels were reached on at least one of these CIs during the test runs. Trends for these two CIs during the 019 experiment are shown in figure 11.

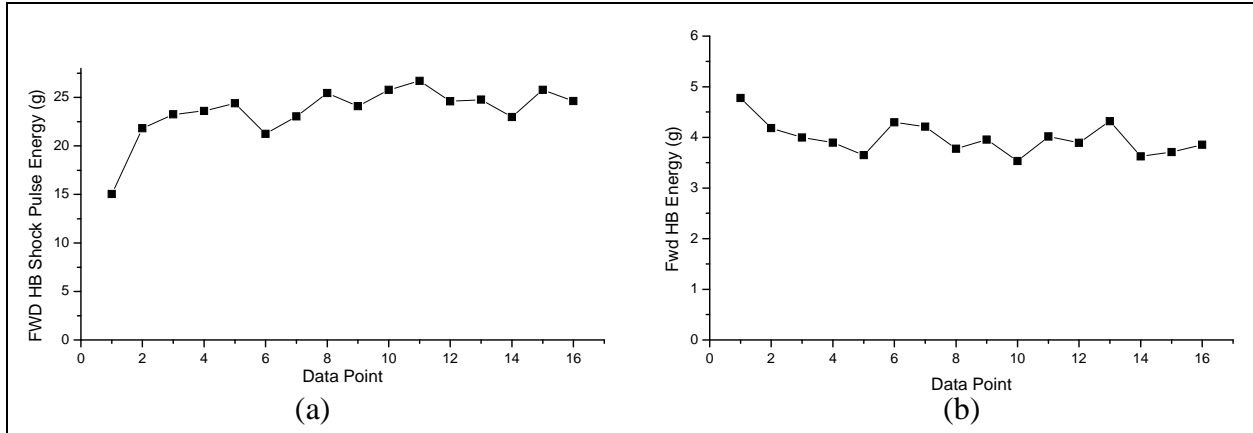


Figure 11. Condition indicator trends for corrosion test 019, (a) shock pulse energy and (b) HB energy.

After the vibration signature tests were completed, one bearing prepared according to each method was disassembled and cleaned in an ultrasonic bath to be able to better inspect and quantify the severity of corrosion damage. The disassembly photographs of 019-ARL-RS are shown in figure 12, and corroborate the pretest visual inspection of the grease and the vibration data. Corrosion damage was found on both races, the cage, and the balls. The inspection of 018-ARL-SW did not show any corrosion damage to the bearing components, as was expected based on the pretest grease visual inspection and the vibration test data.



Figure 12. Photographs of corrosion damage to bearing 019-ARL-RS after post-test disassembly.

### 4.3 Sand Contamination

To investigate the effect of contamination of the bearing with sand, as might occur in the case of a damaged or missing seal, two different grain sizes of sand were mixed into grease of the hanger bearings. The fine sand contaminant chosen was “Arizona test dust,” in accordance with ISO 12103-1 (9), in the range of 0–80 micron particle size and consisting mostly of  $\text{SiO}_2$ . The coarse sand chosen was a commercially available product consisting of mostly  $\text{SiO}_2$  and majority of the volume having particle size in the 100–500 micron range. Both grades of contaminants were mixed into the grease in a proportion of 190 cc of grease to 10 cc of sand. Two bearings were prepared with each type of contaminant, for a total of four test bearings. One vibration signature experiment was performed with each of these bearings, labeled as 011-ARL-CS, 012-ARL-FS, 014-ARL-CS, and 015-ARL-FS, where the –FS designates a fine sand contaminant and the –CS designates a coarse sand contaminant.

Over the course of the 012-ARL-FS test lasting approximately 18 min, the RMS acceleration was found to trend upward for the entire run, with a much more rapid increase near the end before the test was terminated. The torque slowly decreased with time in a manner consistent with the grease heating up during operation. Of the four condition indicators calculated by the VMEP system, only two showed significant responses over the course of the run – the “Fwd HB 1R Vib,” and the “Fwd HB Energy.” The 1R vibration CI increased by about 40% over the duration of the experiment, while the HB energy CI nearly tripled. The time traces of RMS acceleration, torque, and the energy CI over the test are given in figure 13.

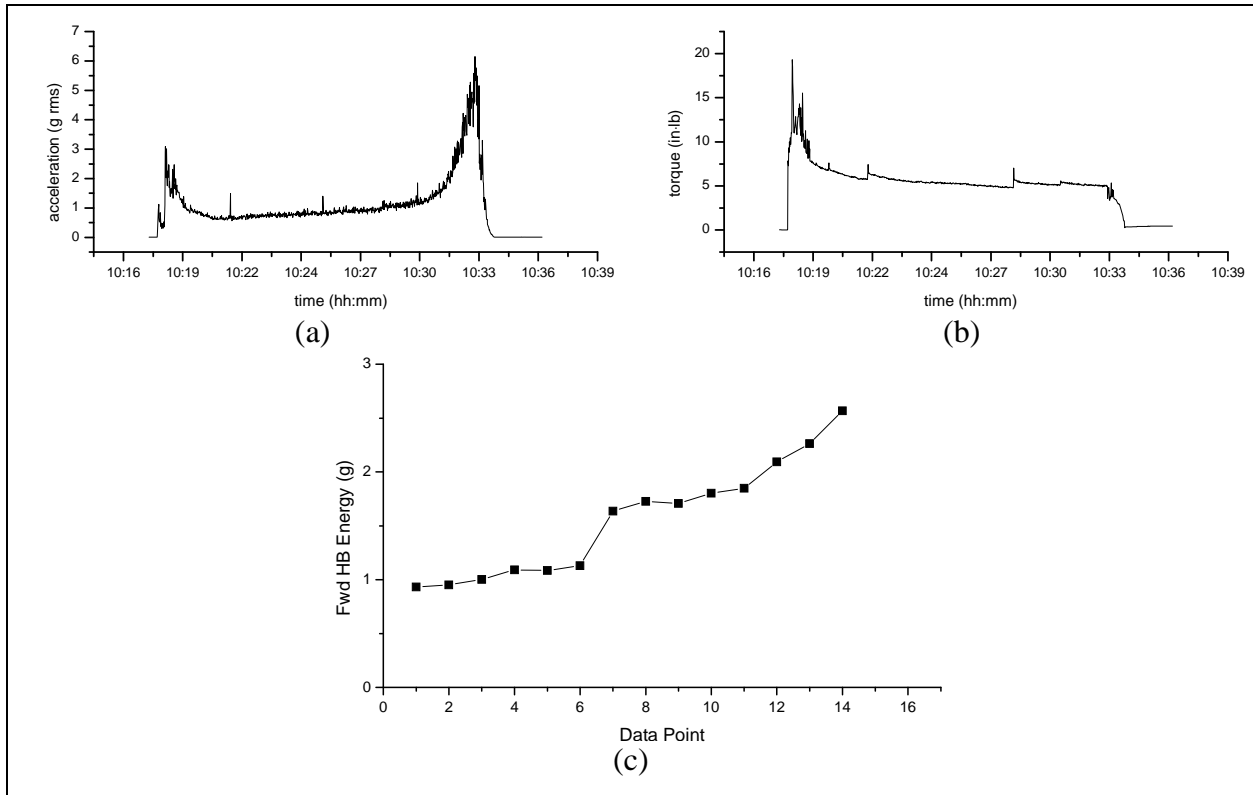


Figure 13. Time traces of (a) acceleration, (b) torque, and (c) HB energy CI, for a test with fine sand (012-ARL-FS).

These vibration characteristics are consistent with wear of the bearing components due to the presence of an abrasive contaminant, and a corresponding increase in the clearance. As the clearance grows, the bearing loses precision and operation becomes rougher. In addition to the broadband RMS vibration and the bearing energy CI, an FFT of the acceleration signal was taken every thirty seconds throughout the duration of the test. As the test progressed, the vibration energy was observed to grow substantially in the range of 4000–6000 Hz, where some natural frequencies of the hanger assembly reside, as discussed in the appendix. Near the end of the 012-ARL-FS run, three of these FFT snapshots are shown in figure 14 to demonstrate the portions of the spectrum where amplitude is increasing.

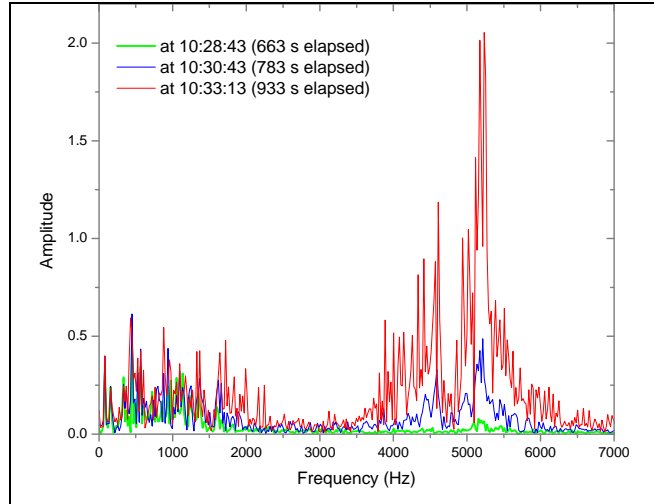


Figure 14. Snapshots of FFT of acceleration signal at several points during 012-ARL-FS (hh:mm:ss in legend)

While the 012 specimen shows the most dramatic change in acceleration behavior at the component level, the time traces of the other three tests are also given in figure 15 to demonstrate the span of behavior observed. It is important to note that the short duration of these experiments do not forecast the long term wear rates of a sand-contaminated bearing, and are intended mostly to demonstrate the resulting vibration signature that may be expected if a bearing were to be contaminated in this way. In the 10–25 min period that these vibration signature experiments were conducted, it is notable that the rate of vibration increase is substantial, and a consequence of the aggressive amount of contaminant seeded into these specimens.

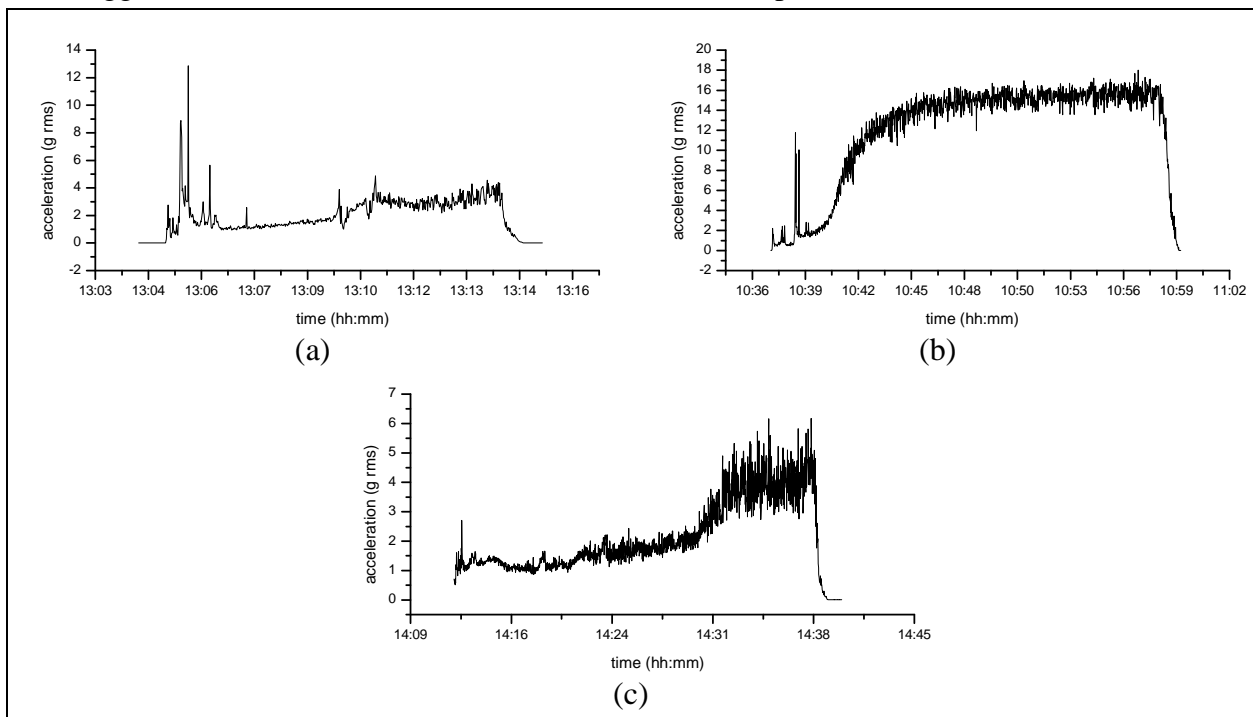


Figure 15. Time traces of broadband RMS vibration for other sand contaminated bearings – (a) 011-ARL-CS, (b) 014-ARL-CS, and (c) 015-ARL-FS

#### 4.4 Other Seeded Faults

Several other fault modes were investigated as part of this seeded fault methodology, but are not discussed in great detail here.

One of the first faults simulated in this study involved using a 1/32" end mill to drill into the ball track of the race, approximately 0.015 in deep, detailed in figure 16. Various configurations of this fault on test specimens were attempted, including a single spall on either inner or outer race, a single spall on both races of a single bearing, and multiple spalls on the inner race. This method of simulating spall damage to a race was found to be less aggressive than required to generate a significant vibration response for the lightly loaded bearing.

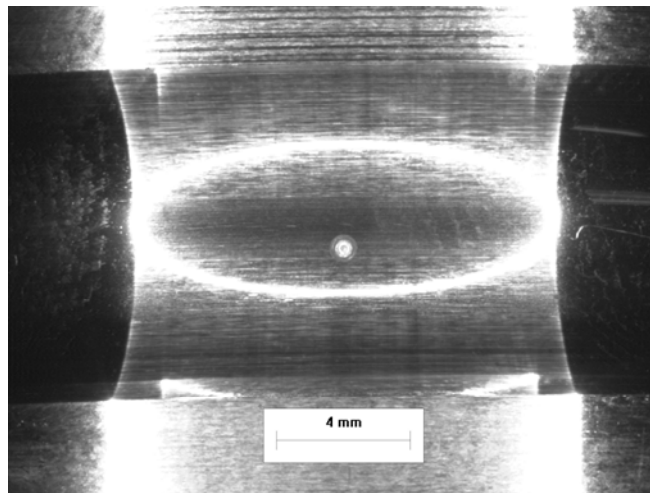


Figure 16. Single simulated spall in center of race.

As time between overhaul (TBO) extensions are considered, another fault mode of particular interest is grease degradation or loss. With longer service lives and reduced inspections, there is an increased possibility that grease quality could degrade or quantity diminish without discovery. The ability for vibration monitoring to detect the gradual loss of grease lubrication is an important question that is being addressed under a separately reported study.

Grease loss can occur if a bearing seal is missing and operating conditions facilitate grease shedding. Several definitions for “low grease” bearings were used, although the vibration response was not nearly as severe as the faults detailed in this report. Because of the light radial load and the short run times, it is thought that in all cases the reduction in grease was not sufficient to substantially impact the bearing operation. Only a very small fraction of the grease charge participates in the lubrication of the ball contacts at any given time, while the rest of the grease charge acts as a reservoir to replace depleted base oil.

Degradation of the grease through mechanical shearing and chemical aging is also a concern for the bearing operation as the period of operation is extended. A separate investigation of grease degradation chemistry and mechanics in this and other bearings in helicopter drivetrains is being

conducted. Figure 17 shows the grease appearance after 1600 hr of run time at light load and high temperature. The increased temperature acts to accelerate the life of the grease, decreasing the required test time. To date, the bearings have operated remarkably well given the severity of lubrication degradation.



Figure 17. Grease appearance after 1600 hr of elevated temperature (accelerated life) operation.

---

## 5. Concluding Remarks

---

To support TBO extension for the AH-64 hanger bearing, a series of baseline and seeded fault vibration experiments was conducted on a component-level rig. Faults investigated included various spall-like race faults, reduced grease, degraded grease, sand-contaminated grease, and salt water corrosion damage. Of these fault modes, it is expected that spallation of the races is very unlikely due to the light loads seen by the bearings on the aircraft. Reduced or degraded grease, as well as contamination and corrosion are thought to be more likely failure modes. While reduced and degraded grease bearing failure mechanisms are reported separately, the vibration response of a forward hanger bearing assembly to several possible faults has been investigated here.

The condition indicators currently used for hanger bearing fault detection on VMEP equipped aircraft did not necessarily exhibit the expected response to various flaw types and sizes, but the component-level test rig has dynamic characteristics that may vary greatly from system-level stands and the actual aircraft. Resonances, structural transfer functions, and forcing functions all influence the dynamic response of the bearing, and the condition indicators programmed and tuned for the aircraft may not be appropriate for a particular component-level stand.

Despite any differences between the component-level tests and the aircraft, it is notable that the increased vibration energy present in the faulted bearings was not always captured by the four tracked condition indicators. This increased energy in the 4000–6000 Hz band was noted for multiple fault modes, including trench-shaped flaws on the bearing inner race, corrosion damage to all components within the bearing, and increased clearance caused by abrasive sand contamination. In all of these cases, vibration energy caused by the respective faults appeared to excite the natural frequency of the hanger assembly, thus influencing the measured vibration and computed CIs. Impact tests in various configurations suggest that these natural frequencies are not heavily dependent on the specific mounting on this test stand, and may be useful in further CI development for this component. It is acknowledged however that the vibration environment on the aircraft may separately produce substantial content in this frequency range, potentially masking these faults.

---

## 6. References

---

1. Keller, J.; et al. Examples of Condition Based Maintenance with the Vibration Management Enhancement Program. *Proceedings of the American Helicopter Society 61<sup>st</sup> Annual Forum*, Grapevine, Texas, 1-3 June 2005.
2. Nenninger, G. Aviation Condition Based Maintenance (CBM). *DoD Maintenance Symposium, Society of Automotive Engineers*, 2007.
3. Brown, R. CBM Program Update DA & OSD Senior Leaders. 30 Nov 2004.
4. Krantz, T.; et al. Summary of Research to Implement CBM for a Grease Lubricated Bearing from the Army's AH-64 Helicopter. *Proceedings of the AHS Specialists' Meeting on Condition Based Maintenance*. American Helicopter Society, 2009.
5. *Operator's Manual for Helicopter, Attack, AH-64D Longbow Apache*; TM 1-1520-251-10
6. *AWR for AH-64D Helicopters Participating in CBM using the VMEP or MPSU*; Airworthiness Release. 21 Oct 2008, Army Aviation Engineering Directorate.
7. *Aviation Unit and Intermediate Maintenance Manual: Helicopter, Attack, AH-64A Apache*; TM 1-1520-238-23.
8. *AH-64A/D Conditioned Based Maintenance (CBM) Component Inspection and Maintenance Manual: Using the Modernized Signal Processor Unit (MSPU) or VMU (Vibration Management Unit)*; Army Aviation Engineering Directorate, 21 Oct 2008.
9. *Road Vehicles – Test Dust for Filter Evaluation – Part 1: Arizona Test Dust*; ISO Standard 12103-1, First Edition, International Organization for Standardization, 1997.

---

## Appendix. Natural Frequency Identification in the Hanger Assembly

---

Following the series of hanger bearing seeded fault tests where vibration amplitude increased in the 4000–6000 Hz range for multiple faults, a series of impact tests were performed on the assembly while the shaft was not rotating in order to identify system natural frequencies and their dependence on the test rig configuration. Vibration spectra on faulted hanger bearings showed large amplitude response in the range of 4000–6000 Hz, a range not addressed by currently monitored CIs. The impact tests performed on the hanger assembly suggest that there are natural frequencies at ~4500 Hz and ~5000 Hz that are relatively independent of the hanger assembly base mounting and the rig shaft. Comparing the responses of the assembly with the shaft and hanger bearing installed versus the responses when these components have been removed shows little effect on the natural frequencies of the system, verifying that these are characteristics of the hanger assembly itself. Instrumentation and impact orientations are shown below.

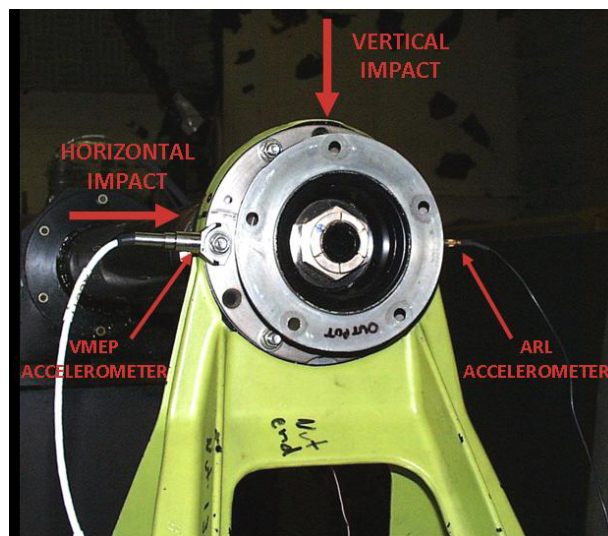
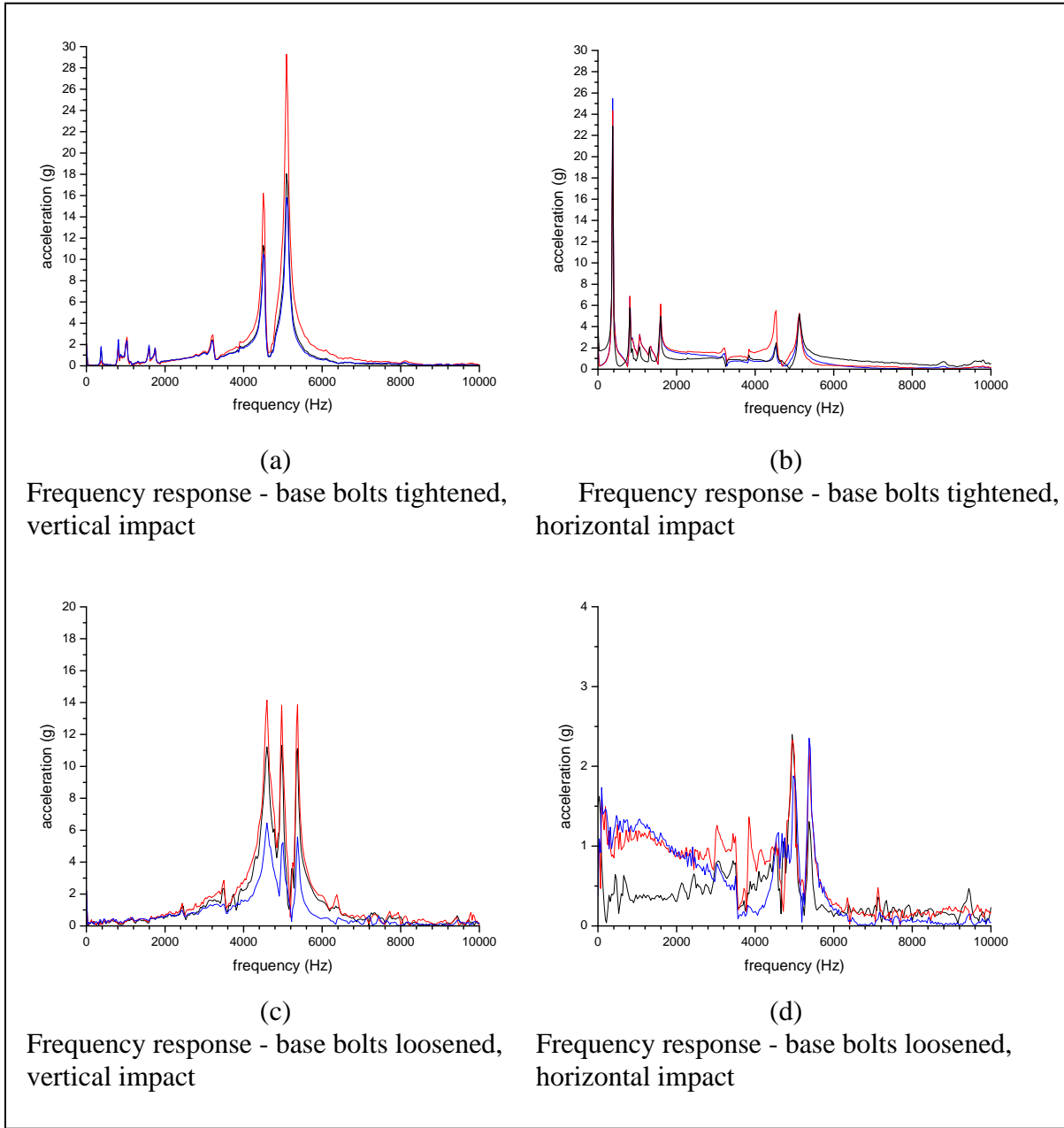


Diagram showing location of accelerometers and directions of impacts for natural frequency identification in the hanger assembly.

Frequency domain response to impact tests with the hanger bearing and shaft removed (hanger assembly only) are shown in (a)–(d) below. Both horizontal and vertical impacts are performed with the hanger assembly bolted down, and again with the bolts loosened. Three impacts were performed in each configuration and are shown plotted together in different colors. Large amplitude response indicates natural frequencies at ~4500 Hz and ~5000 Hz, irrespective of impact orientation or base constraint (bolted/unbolted). The presence of these peaks in these impact tests suggests that the rig shaft and hanger bearing also have little influence on these natural frequencies, and they appear to be inherent to the hanger assembly itself. When the bolts

are loosened the assembly also shows a peak at ~5350 Hz. Peaks at ~ 350, ~825, and ~1650 Hz have large amplitudes for the horizontal impacts when the base is bolted, but disappear into a broad energy distribution for the unbolted case, suggesting that these natural frequencies are dependent on the rig mounting, and that these modes may involve the entire stand and assembly cantilevered from its attachment to the rig base.



---

## List of Symbols, Abbreviations, and Acronyms

---

CBM	condition-based maintenance
CI	Condition Indicators
EDM	electric discharge machining
FFT	fast Fourier transform
RMS	root mean square
TBO	time between overhaul
VMEP	Vibration Management Enhancement Program

NO OF. COPIES	ORGANIZATION	NO OF. COPIES	ORGANIZATION
1 ELEC	ADMNSTR DEFNS TECHL INFO CTR ATTN DTIC OCP 8725 JOHN J KINGMAN RD STE 0944 FT BELVOIR VA 22060-6218	1 HC	ODIR, VHCL TCHNLGY ATTN RDRL VT B SELJAN BLDG 501 RM 233 21000 BROOKPARK RD CLEVELAND OH 44135-3191
1 HC	DARPA ATTN IXO S WELBY 3701 N FAIRFAX DR ARLINGTON VA 22203-1714	1 HC	NASA GLENN ATTN RDRL VTP D LEWICKI BLDG 23 RM W119A CLEVELAND OH 44135-3191
1 CD	OFC OF THE SECY OF DEFNS ATTN ODDRE (R&AT) THE PENTAGON WASHINGTON DC 20301-3080	1 HC	NASA GLENN ATTN RDRL VTP H DECKER BLDG 23 RM W121 CLEVELAND OH 44135-3191
1 HC	US ARMY RSRCH DEV AND ENGRG CMND ARMAMENT RSRCH DEV AND ENGRG CTR ARMAMENT ENGRG AND TECHNLGY CTR ATTN AMSRD AAR AEF T J MATTS BLDG 305 ABERDEEN PROVING GROUND MD 21005-5001	1 HC	NASA GLENN ATTN RDRL VTP T KRANTZ BLDG 23 RM W115 CLEVELAND OH 44135-3191
1 HC	PM TIMS, PROFILER (MMS-P) AN/TMQ-52 ATTN B GRIFFIES BUILDING 563 FT MONMOUTH NJ 07703	1 HC	US GOVERNMENT PRINT OFF DEPOSITORY RECEIVING SECTION ATTN MAIL STOP IDAD J TATE 732 NORTH CAPITOL ST NW WASHINGTON DC 20402
1 HC	US ARMY RSRCH LAB ATTN RDRL CIM G T LANDFRIED BLDG 4600 ABERDEEN PROVING GROUND MD 21005-5066	1 HC	US ARMY RSRCH LAB ATTN RDRL CIM G T LANDFRIED BLDG 4600 ABERDEEN PROVING GROUND MD 21005-5066
1 HC	US ARMY INFO SYS ENGRG CMND ATTN AMSEL IE TD F JENIA FT HUACHUCA AZ 85613-5300	1 HC	DIRECTOR US ARMY RSRCH LAB ATTN RDRL ROE V W D BACH PO BOX 12211 RESEARCH TRIANGLE PARK NC 27709
1 HC	COMMANDER US ARMY RDECOM ATTN AMSRD AMR W C MCCORKLE 5400 FOWLER RD REDSTONE ARSENAL AL 35898-5000	3 HC	US ARMY RSRCH LAB ATTN RDRL CIM P TECHL PUB ATTN RDRL CIM L TECHL LIB ATTN IMNE ALC HRR MAIL & RECORDS MGMT ADELPHI MD 20783-1197
20 HC	NASA GLENN ATTN RDRL VTP B DYKAS BLDG 05 RM W213B CLEVELAND OH 44135-3191		
		TOTAL: 37 (1 ELEC, 1 CD, 35 HCS)	